IEEE Access
Multidisciplinary ⋮ Rapid Review ⋮ Open Access Journal

Received 10 October 2025, accepted 21 October 2025, date of publication 28 October 2025, date of current version 21 November 2025.

Digital Object Identifier 10.1109/ACCESS.2025.3625653

RESEARCH ARTICLE

Compact Quad-Port MIMO Antenna Employing Defected Substrate and Ground Plane for Sub-6 GHz 5G Communication

BHASKARA RAO PERLI[1], TATHABABU ADDEPALLI[2], MANUMULA SRINUBABU[2], SIVASUBRAMANYAM MEDASANI[3], (Senior Member, IEEE), PADMAJA NIMMAGADDA[4], C. RAJU[5], MANISH SHARMA[6], (Senior Member, IEEE), ZAHRILADHA ZAKARIA[7], (Senior Member, IEEE), AND AHMED JAMAL ABDULLAH AL-GBURI[7], (Senior Member, IEEE)

[1]Department of ECE, St. Ann's College of Engineering and Technology, Chirala, Andhra Pradesh 523187, India
[2]Department of ECE, Aditya University, Kakinada, Andhra Pradesh 533437, India
[3]Department of CSE, K. S. School of Engineering and Management, Bengaluru 560109, India
[4]Department of ECE, Mohan Babu University (Erstwhile Sree Vidyanikethan Engineering College), Tirupati, Andhra Pradesh 517102, India
[5]Department of ECE, Sri Venkateswara College of Engineering, Tirupati, Andhra Pradesh, India
[6]Chitkara University Institute of Engineering and Technology, Chitkara University, Punjab 140417, India
[7]Center for Telecommunication Research and Innovation (CeTRI), Fakulti Teknologi dan Kejuruteraan Elektronik dan Komputer (FTKEK), Universiti Teknikal Malaysia Melaka (UTeM), Durian Tunggal, Melaka 76100, Malaysia

Corresponding author: Zahriladha Zakaria (zahriladha@utem.edu.my)

This work was supported in part by the Universiti Teknikal Malaysia Melaka (UTeM), in part by the Centre for Research and Innovation Management (CRIM), and in part by the Ministry of Higher Education of Malaysia (MOHE).

ABSTRACT This work presents a low-profile, compact quad-port MIMO antenna structure optimized for sub-6 GHz and X-band wireless communication. The antenna employs a tapered and stepped monopole radiator in conjunction with defected substrate and ground plane modifications to enhance isolation, improve diversity performance, and support dual-band operation. A single monopole element, designed on an FR-4 substrate ($\varepsilon_r = 4.3$, $\tan\delta = 0.002$), has been extended into a quad-port configuration with orthogonally oriented ports to achieve polarization diversity and minimize mutual coupling. Although the spacing is less than $\lambda_{max}/2$ ($0.14\ \lambda_0$), a reduced inter-element gap of 11.25 mm is adopted to achieve compact integration. The antenna measures $44 \times 44 \times 1.6$ mm^3 and operates across two frequency bands: 2.75–4.4 GHz and 10.33–13 GHz (S_{xx} < -10 dB) with S_{xy} values below –17.5 dB and –25 dB in the respective bands, ensuring robust MIMO performance. With its compact design and efficient radiation characteristics, the proposed antenna is well-suited for 5G-NR systems, IoT devices, V2X communication, and satellite-based applications.

INDEX TERMS Multiple-input multiple-output (MIMO), compact size, defected substrate and ground, tapered and stepped antenna, dual band, 5G and X-band.

I. INTRODUCTION

The increasing demand for high-speed and reliable wireless links in emerging technologies has accelerated the development of multi-band antenna systems. These are especially vital for next-generation networks such as 5G New Radio (NR), operating in both the sub-6 GHz and X-band regions. Applications across these spectra include broadband satellite platforms like direct-to-home broadcasting, MSS, and FSS. The proposed antenna addresses such requirements through a compact multi-port design that maintains compliance with ITU standards while supporting efficient data throughput. Moreover, it is envisioned for deployment in diverse domains, including smart infrastructure, vehicular networks, and satellite nodes [1], [2], [3], [4]. Real-time application scenarios of the proposed quad-port MIMO

The associate editor coordinating the review of this manuscript and approving it for publication was Tutku Karacolak.

antenna, demonstrating its integration in smart home, automotive, and satellite communication systems s shown in Fig. 1. With the rapid evolution of 5G and X-band services, there is a significant increase in system bandwidth and capacity requirements. To address this requirement, sophisticated MIMO antenna systems are employed to improve spatial diversity and increase data transmission capacity. Recent MIMO designs emphasize low-profile printed antennas integrated with defected ground structures (DGS) for dual-band operation [3], [5], [6]. Such configurations are pivotal in applications spanning smart services, automation, healthcare, and IoT. Furthermore, monopole-based antennas are widely employed due to their small form factor, wide impedance bandwidth, and cost-effectiveness [3], [7]. The operation within sub-6 GHz bands, such as n77/78/79/80, and 5G Wi-Fi bands requires antenna arrays that maintain compactness while delivering high isolation, gain, and efficiency [5], [8], [9], [10]. MIMO systems are instrumental in improving link reliability and spectral efficiency, though increased element count or reduced inter-element spacing leads to mutual coupling, negatively affecting system performance [3], [11], [12], [13], [14], [15]. Various techniques are proposed to reduce mutual coupling in MIMO antenna systems, such as the use of defected ground structures (DGS), electromagnetic band gap materials, metamaterials, neutralization lines, decoupling circuits, dielectric resonator elements, and reconfigurable components [2], [5], [6], [10], [12], [15], [17], [18], [19], [20], [21], [22], [23], [24], [25], [26], [27]. Among these methods, DGS has demonstrated significant effectiveness by altering the surface current flow, attenuating surface wave propagation, and lowering unwanted electromagnetic interaction between radiating elements. This approach enhances port-to-port isolation while preserving the compact nature of the antenna configuration.

FIGURE 1. Real-time application scenarios of the MIMO antenna system, demonstrating its integration in smart home, automotive, and satellite communication systems.

Various antenna architectures have been proposed to meet the compactness and performance requirements. A 55 × 55 × 1 mm^3 MIMO antenna, for instance, achieved an isolation level of –20 dB across 3.09–3.7 GHz, utilizing frequency selective surfaces and orthogonal element arrangements [28]. Another model measuring 56 × 56 × 0.1 mm^3 supported tri-band operation but exhibited challenges in optimizing spacing for isolation [29]. An antenna design measuring 77 × 70.11 × 1.6 mm^3 operated within the frequency range of 4.53–4.97 GHz, delivering around 5 dB average gain and maintaining radiation efficiency between 60% and 80% [30]. Another compact dual-band structure, sized at 50 × 42 × 1.6 mm^3, supported two bands, 2.80–4.20 GHz and 6.10–9.0 GHz, with an inter-element distance of 9 mm, isolation close to 18 dB, and efficiency reaching 82.4% [31]. Other studies explored DGS-enhanced antennas with sizes between 62 × 52 × 0.25 mm^3 and 68 × 68 × 1.6 mm^3, utilizing vertical stubs and decoupling elements to achieve isolation below –23 dB [18], [32]. Antennas ranging from 55 × 55 × 1.6 mm^3 to 34 × 129 × 1.6 mm^3 also integrated parasitic loops, L-slots, and decoupling structures to improve isolation, though challenges in maintaining a unified ground structure and overall miniaturization persist [6], [33]. Additionally, a four-port configuration of 65 × 90 × 1.6 mm^3 incorporated DGS for multiband operation across 1.9 GHz to 5.5 GHz, maintaining mutual coupling (S_{xy} =15 dB) and an ECC under 0.5 [34]. In [45], a compact 56 × 56 × 1.6 mm^3 square-shaped SRR-based fractal antenna covers 1.75–2.00 GHz (13.36%) and 3.01–4.18 GHz (33.42%), achieving >1.80 dBi gain, >80% efficiency, and 2:1 VSWR bandwidths of 620 MHz and 580 MHz for GSM and sub-6 GHz indoor repeater use. In contrast, [46] reports a 60 × 60 × 11.6 mm^3 quad-port design employing aperture-coupled feeding and DRA, yielding S_{21} of −20/−26 dB, gains of 5.8/6.2 dBi, fractional bandwidths of 18.7%/14.6%, and efficiencies of 88.6%/90.2%, with the DRA substantially lowering mutual coupling.

To overcome existing challenges, this work proposes a compact four-port tapered and stepped dual-wideband MIMO antenna with dimensions of 44 × 44 × 1.6 mm^3. The chosen footprint balances compactness with the requirements of a novel four-port, dual-band, unified-ground MIMO design. At the lowest band (∼3.4 GHz), the $\lambda_0/2$ element spacing is ∼40 mm, but our design compresses this dimension to 11.25 mm (∼0.14 λ_0) without compromising performance. Such compactness is achieved through an orthogonal element arrangement combined with self-coupled defected ground structures (DGS), grounding branches, and stubs that actively control surface currents to enhance isolation and maintain very low ECC. Unlike many smaller antennas that often operate in a single band, use separate grounds, or rely on bulky decoupling networks, our shared-ground design achieves wide dual-band coverage (2.72–4.45 GHz and 10.33–13 GHz) with S_{21} better than −16 dB and −25 dB for the respective bands. It maintains stable gain, high efficiency and robust diversity performance.

To overcome existing challenges, this work proposes a compact four-port tapered and stepped dual-wideband MIMO antenna with overall dimensions of 44 × 44 × 1.6 mm^3. The selected footprint provides an optimal balance between compactness and the functional requirements of a novel four-port, dual-band, unified-ground MIMO configuration. At the lowest resonance band (≈ 3.4 GHz), the theoretical

$\lambda_0/2$ element spacing is approximately 40 mm, while the proposed design effectively compresses this dimension to 11.25 mm ($\approx 0.14\lambda_0$) without compromising electromagnetic performance. This high level of miniaturization is achieved through an orthogonal element arrangement integrated with self-coupled defected ground structures (DGS), grounding branches, and slit-loaded stubs. Collectively, these features enhance port isolation, regulate surface current distribution, and maintain very low envelope correlation coefficient (ECC) values. Unlike many compact MIMO antennas that suffer from single-band limitations, separate ground planes, or bulky decoupling networks, the present shared-ground design achieves dual-wideband performance covering 2.72–4.45 GHz and 10.33–13 GHz with S_{21} isolation better than –16 dB and –25 dB, respectively. The antenna further exhibits stable gain, high radiation efficiency, and robust diversity characteristics across the operational bands.

II. DESIGN METHODOLOGY OF THE PROPOSED ANTENNA

The design progression of the antenna is detailed in this section, along with an analysis of its response under varying conditions. The subsequent sections provide a comprehensive and organized overview of the design approach applied to both the refined single-element antenna and the newly introduced four-port MIMO configuration.

A. TAPERED AND STEPPED MONOPOLE ANTENNA

Figure 2 illustrates the progressive design stages of the tapered and stepped monopole antenna, realized on an FR-4 substrate ($\varepsilon_r = 4.3$, $\tan\delta = 0.002$) with a thickness of 1.6 mm. The antenna evolves through five configurations (Ant. 1–Ant. 5), each incorporating structural modifications to enhance impedance matching, bandwidth, and dual-band performance.

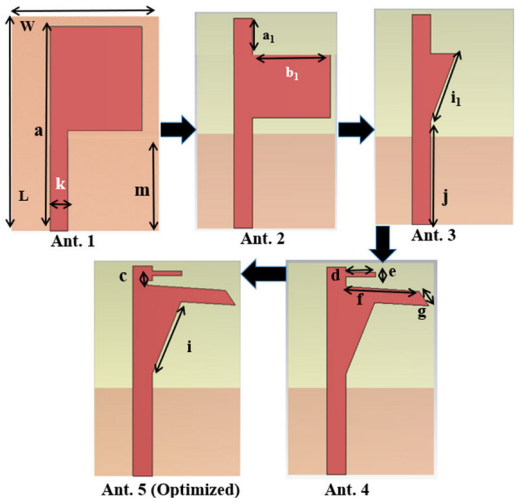

FIGURE 2. Evolution of Single Monopole Antennas [a=21.50, a1=4, b1=9, b=2, c=2, d=3, e=0.5, f=8, g=1.8, i=8, j=10.50, k=2, w=15, L=22, all are in mm.]

The initial configuration (Ant. 1) employed a basic rectangular monopole measuring 22 × 15 mm^2, fed by a 2 mm microstrip line of electrical length 21.50 mm and supported by a full ground plane. In Ant. 2, a rectangular slot of dimensions ($a_1 \times b_1$) was etched into the radiator, and the ground plane was reduced to a partial length of 9 mm. This modification enabled excitation in the lower sub-6 GHz band; however, the impedance matching at resonance was limited to –12 dB, restricting effective bandwidth. To enhance dual-band capability, Ant. 3 adopted a triangular-tapered radiator with diagonal length i_1. This geometry introduced resonances at 3.80 GHz and 12.50 GHz with return losses of –14.1 dB and –18.25 dB, respectively. While compact and structurally efficient, the design provided limited bandwidth and moderate matching.

Ant. 4 incorporated further refinements, including a horizontal stepped extension and multiple slots (dimensions d, e, f, and g) in the radiator. These features broadened the bandwidth, improved impedance matching, and strengthened isolation in MIMO operation. The horizontal extension acted as a capacitive load to tune the resonant frequency, while the slits and slots generated additional resonances. This configuration achieved stable operation in the mid-band 5G-NR spectrum, with resonance at 3.4 GHz ($|S_{11}| = -35$ dB) and extended coverage beyond 13 GHz.

The optimized design (Ant. 5) integrated a defected ground structure (DGS) and refined radiator geometry. A 0.5 × 0.5 mm^2 square slit was introduced at the top of the horizontal extension, while the triangular diagonal was shortened to i = 8 mm, improving current distribution and resonance tuning. As a result, Ant. 5 exhibited broad frequency coverage with strong resonances at 3.45 GHz ($|S_{11}| = -35$ dB) and 11.5 GHz ($|S_{11}| = -42.5$ dB). The synergy of tapered profiling, stepped modifications, and DGS integration enabled dual-band operation over 2.72–4.45 GHz and 10.33–13 GHz, achieving excellent impedance matching and wide bandwidth in a compact form factor suitable for four-port MIMO implementation.

In addition, the radiator includes a rectangular slot with a length 'f' and a diagonal width 'g'. This design adjustment is implemented to improve the bandwidth and antenna's resonance. The integration of stepped and extended features contributes to bandwidth enhancement and enables reliable dual-band functionality. The horizontal extension acts as a capacity load, aiding in the adjustment of the resonant frequency, while the slits and slots introduce new resonances that improve isolation in MIMO configurations. The antenna operates effectively within the sub-6GHz mid-band spectrum, particularly the n77/78/79/48 5G-NR bands. It initiates operation at 3.4 GHz and achieves a minimum $|S_{11}|$ of −35 dB, demonstrating superior impedance matching performance. A higher frequency band is achieved beyond 13 GHz.

The synergy of tapered profiling, stepped design features, and finely tuned dimensions facilitates effective realization of a four-port MIMO system. As illustrated in Fig. 3, the optimized tapered-stepped monopole is expanded into a quad-port MIMO arrangement, maintaining a compact form factor with overall dimensions of N × N mm^2. The

antenna elements are orthogonally positioned with uniform inter-element spacing (Gap) to achieve both pattern and polarization diversity. This configuration improves isolation and extends the operational bandwidth. The overall MIMO design maintains a compact footprint of 44 × 44 × 1.6 mm^3. According to the $\lambda_{max}/2$ criterion at 3.8 GHz, the theoretical spacing between elements is approximately 40 mm, as expressed in (1). Each radiating element is realized on a shared substrate with individual ground planes. Intra-elements are separated by 11.25 mm. This structural arrangement ensures compact integration along with dual-band functionality and efficient impedance matching.

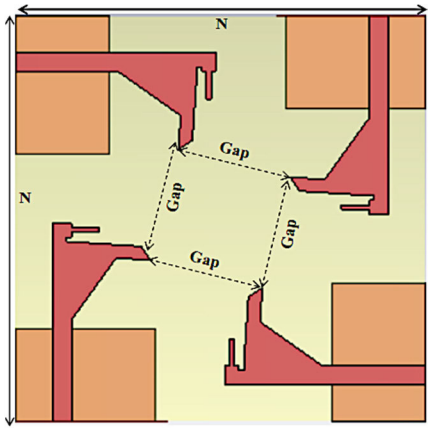

FIGURE 3. Quad-port MIMO antenna configuration with individual ground.

$$Gap = \frac{4\pi}{4\pi * \left(1 - 10^{\frac{l_{max}}{10}}\right)} = \frac{\lambda_{max}}{2} \quad (1)$$

$\lambda_{max.}$ = C/f (mm), here C= speed of light (3×10^8m/s) and f= f (GHz) is operating frequency then

$$= 300.0/3.80 = 78.949 \text{ mm}$$
$$\lambda_{max}/2 = 78.976/2 = 39.74 = 40 \text{ mm}$$

Using (2) includes the C_c, which measures the coupling between antennas (I, &j,).

$$\left|C_{coupling}\right|^2 = \frac{S_{21(j,)}}{\sqrt{((1-|S_{11}|^2)(i,) * (1-|S_{22}|^2(j,))}}) \quad (2)$$

The simulated S-parameters indicate an S_{21} value of −15.5 dB within the operating frequency band, demonstrating adequate isolation between antenna elements.

$$|C_c|^2 = S_{21mag} * exp^{S21phase} = 0.16778$$

S_{21}(j) denotes the transmission parameter from element j to element i, characterizing inter-port signal coupling. The reflection coefficients S_{11}(i) and S_{22}(j) represent the input and output return losses at antenna elements i and j, respectively and C_c = coupling. These parameters are essential for evaluating the impedance matching and isolation performance between ports. The mutual isolation (I) between two antenna elements is determined using (3).

$$I = 20\log_{10}\left(\frac{1}{\sqrt{\left(1 - |S_{ij}|^2\right)}}\right) \quad (3)$$

$$I = -20\log_{10}\left(|C_c|^2\right) = -20\log_{10}(0.167788) = -15.45dB$$

In the development of the antenna, several structural modifications were applied to both the substrate and ground regions, as illustrated in Fig. 4(a). A rectangular slit measuring 17.57 mm × 3.85 mm ($c_1 \times d_1$) is introduced at the center of each edge. Additionally, slits of 6 mm × 1 mm ($e_1 \times f_1$) are etched onto all ground planes, and a sub-slot of 2.5 mm × 1 mm is added near the ground edge. These features contribute to downward shifting of the resonant frequencies and improved impedance matching, resulting in return loss values below −10 dB across both bands. The structure exhibits enhanced isolation relative to earlier designs. Furthermore, a vertical rectangular slot 5 mm × 1 mm ($h_1 \times f_1$) is embedded in the shared ground, as shown in Fig. 4(b), further improving the impedance bandwidth in both low- and high-frequency regions. The antenna achieves extended impedance bandwidths with reflection coefficients of −42.5 dB at 3.42 GHz and −23.86 dB at 11.06 GHz. Figure 5(a) shows the top view of the optimized quad-port MIMO antenna, while Fig. 5(b) illustrates the bottom view, emphasizing the grounded stubs that facilitate the shared-ground arrangement. The bent stub measures 3 mm (V) and 4 mm (U) in length, with a width of f_1 (1 mm). Although the configuration includes individual grounds for the MIMO elements, [35] emphasizes the necessity of a common ground for proper MIMO functionality without compromising bandwidth or isolation. The proposed design addresses the challenge of achieving high isolation in a compact structure.

The enhancement incorporates orthogonal element placement, a shared ground plane, and microstrip feeding to improve isolation, bandwidth, and diversity, rendering the design suitable for sub-6 GHz 5G-NR applications.

Figure 6 illustrates the simulated surface current density (SCD) distribution for the proposed quad-port MIMO antenna when Port 1 is excited and the remaining ports are terminated with 50 Ω loads. At 3.15 GHz (Fig. 6a, sub-6 GHz band), the current is strongly concentrated along the feedline, radiator edges, and the adjacent ground region of the excited port. Limited current is observed near the other ports, indicating effective suppression of surface wave propagation across the shared ground. This localized current flow minimizes mutual coupling, which is reflected in the measured S_{21} isolation of better than −15 dB in the lower band.

At 11.95 GHz (Fig. 6b, X-band), the current distribution remains confined to the active radiating element and its immediate ground section, with negligible current leakage toward the inactive elements. This strong confinement at higher frequencies is due to the optimized radiator geometry and defected ground structure (DGS), which disrupts surface currents along the ground plane. As a result, the antenna

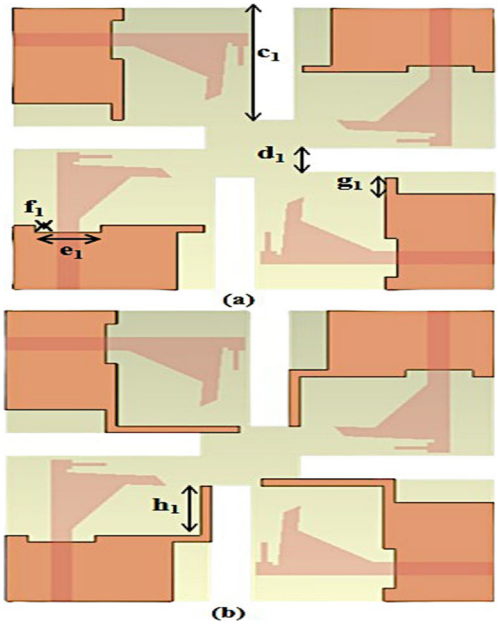

FIGURE 4. Quad-element MIMO antenna incorporating (a) altered substrate and ground plane and (b) vertical stub incorporated into the ground, featuring individual grounds.

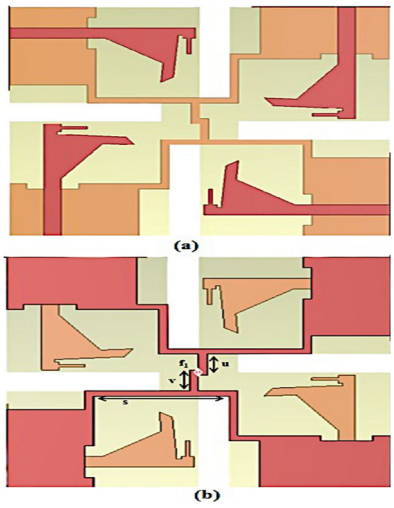

FIGURE 5. (a) Top and (b) bottom configurations of the proposed quad-port MIMO antenna incorporating a unified ground system.

achieves high isolation near −26 dB in the X-band, reducing mutual interference and improving MIMO performance. The DGS plays a pivotal role in breaking the continuous current path in the shared ground, thereby reducing coupling and preserving isolation in both low- and high-frequency bands. This ensures stable radiation behavior, enhanced diversity performance, and minimal degradation in a multiport operation.

III. RESULTS AND DISCUSSIONS

Fig. 7 shows the simulated S_{11} response illustrating the design evolution of the tapered and stepped monopole antenna. Ant. 1, featuring a fundamental rectangular layout, offers a bandwidth of 3.04 GHz ranging from 3.21 GHz to 6.25 GHz,

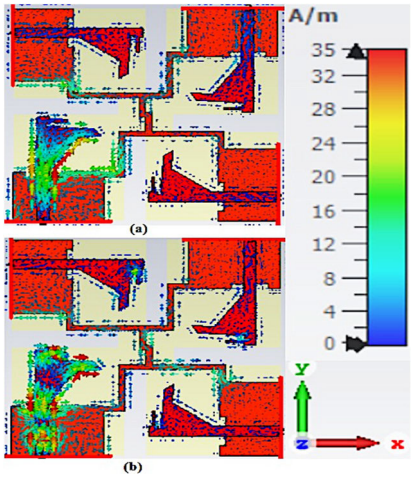

FIGURE 6. SCD of the quad-port MIMO antenna: (a) at 3.15 GHz and (b) at 11.59 GHz for the proposed design.

with a resonance at 4.78 GHz and a corresponding return loss of −25.53 dB. While it effectively covers the lower sub-6 GHz range, it lacks resonance at higher frequencies. Ant. 2 improves on this by extending the lower band to 3.61–6.345 GHz (2.75 GHz bandwidth) at 4.08 GHz with -12.33 dB S_{xx} and introducing a higher band from 12.10 GHz to above 13 GHz, resonating at 12.80 GHz with -21.4 dB S_{xx}. Further refinements in Ant. 3 achieve a broader lower band of 3.41 GHz (3.57–6.98 GHz) at 4.02 GHz with -13.5 dB S_{xx} and a higher band from 11.33 GHz to above 13 GHz, resonating at 12.25 GHz with -18.45 dB of S_{xx}. Ant. 4 provides a more focused lower band with 1.66 GHz bandwidth at 3.54 GHz and -30.36 dB of S_{xx}, along with a higher band spanning 11.74 GHz to above 13 GHz, resonating at 12.89 GHz with -44.95 dB of S_{xx}. The final optimized design, Ant. 5, delivers superior dual-band performance, covering the lower band from 3.04–4.62 GHz (1.58 GHz bandwidth) at 3.45 GHz with -34.59 dB of S_{xx} and the higher band from 10.75–12.75 GHz, resonating at 11.45 GHz with -43.4 dB of S_{xx}. The optimized stepped and tapered single antenna is well suited for sub-6 GHz applications, including n77/n78/n79/n48 bands, and is ideal for satellite communication and effective for modern communication needs. According to the simulated S_{11} results, an optimal feed width of $k = 2$ mm was achieved. Fig. 8(a) displays the corresponding results. The impact of varying the partial ground height 'm' is shown in Fig. 8(b), where 'm' ranges from 8 mm to 10 mm in the simulation analysis. Based on the analysis of the S_{11} performance, $m = 9$ mm is identified as the optimal height, providing excellent impedance matching and ensuring coverage of the desired frequency bands.

As illustrated in Fig. 9(a), the simulated S_{11} response of the stepped rectangular patch antenna demonstrates the effect of varying the length 'f' from 7.5 mm to 8.5 mm and the tapered width 'g' from 1 mm to 2.5 mm. The optimal values are found to be "f" = 8 mm and "g" = 1.8 mm. These optimized parameters ensure the desired dual-band operation, achieving good impedance matching and maintaining a compact size

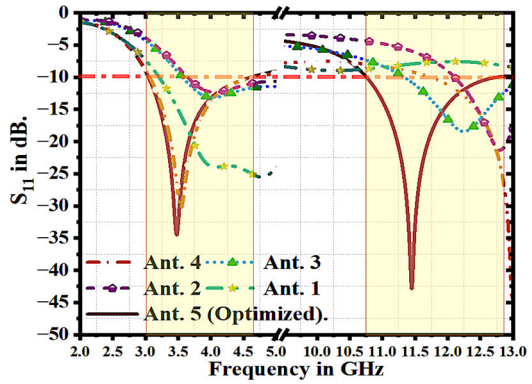

FIGURE 7. Simulated results of the single tapered and stepped monopole antenna evolution.

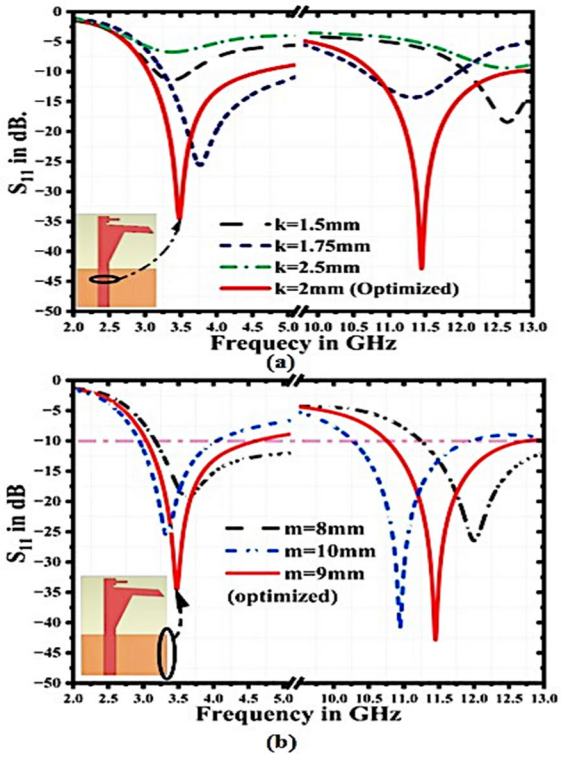

FIGURE 8. Simulated parametric results for the single tapered and stepped monopole antenna: (a) feed width (k), (b) partial ground length (m).

for the single monopole antenna. With optimized parameter values, the antenna achieves effective operation in the lower frequency band of 3.04–4.6 GHz, exhibiting a resonance at 3.45 GHz with an S_{11} of −34.6 dB. In the higher band, it covers 10.76–12.72 GHz, achieving excellent impedance matching with a S_{xx} value of -43.45 dB. The simulated results for the tapered triangular diagonal length (i), as shown in Figure 9(b), indicate that "i" ranging between 7.5 mm to 8.5 mm. Based on the analysis of the S_{11} performance, "i" = 8 mm is identified as the optimal value, providing excellent impedance matching and ensuring coverage of the desired frequency bands.

The optimized set k = 2.0 mm, m = 9 mm, f = 8.0 mm, g = 1.8 mm, i = 8.0 mm yields the broadest dual-band

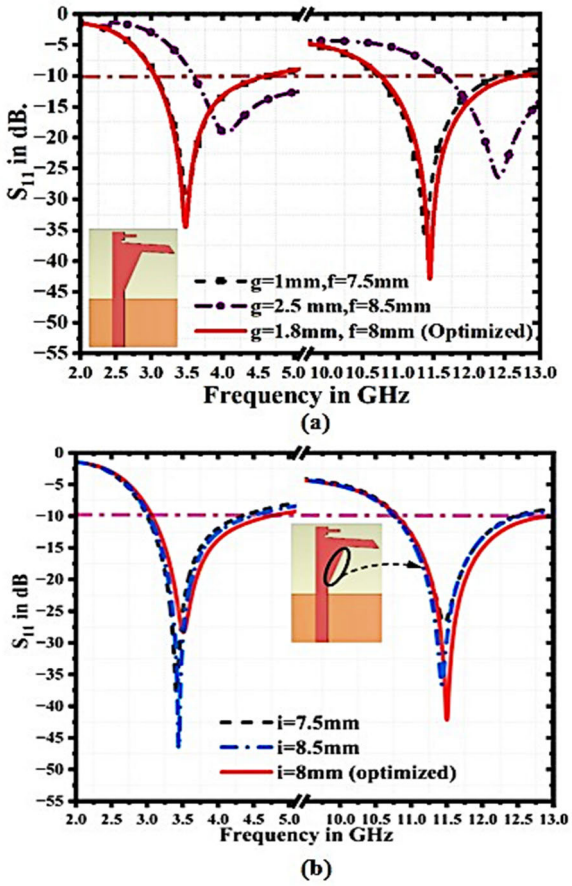

FIGURE 9. Simulated parametric results for the single tapered and stepped monopole antenna: (a) stepped rectangular length (g) and width (f), and (b) tapered triangle diagonal (i).

coverage (2.72–4.45 GHz and 10.33–13 GHz) with deep minima ($|S_{11}|$−34.6 dB at 3.45 GHz; −43.4 dB at 11.45 GHz) while maintaining a compact geometry.

Figure 10 depicts the simulated S-parameters (S_{xx} and S_{xy}) of the 4-port MIMO antenna featuring orthogonal element orientation and isolated ground planes. This configuration achieves a compact design while targeting the desired operating bands. The lower operating band spans from 2.92-5.25 GHz at 4.4 GHz and an S_{xx} value of -18.25 dB, indicating

less impedance matching. The higher operating band ranges from 11.02 GHz to above 13 GHz, resonating at 12.09 GHz with an S_{xx} value of -24 dB. The isolation (S_{xy}) spanning -15 to -18 dB, and -27.5 dB at corresponding bands.

The simulated S_{xx} and S_{xy} parameter results for the defected substrate and DGS are shown in Figure 11(a). These structures influence the sub-6GHz, while the higher non-resonating band spans from 10.60 GHz to 13 GHz, with a resonance at 11.46 GHz and an S_{xx} value of -33.65 dB. The mutual coupling (S_{21}) in the higher band remains between -26.65 dB and -34.25 dB across the entire range Fig. 11(b) depicts the simulated S-parameters (S_{xx} and S_{xy}) for the design incorporating a vertical slot within the ground plane. The S_{xx} response indicates a lower band coverage from

TABLE 1. Different geometric parameters influence the antenna performance.

Parameter	Values Tested	Primary Role	Observed Trend on S_{11} / Bands	Optimized Value	Impact
Feed width k (mm)	1.5, 1.75, 2.0, 2.5	Input impedance at low band	1.5–1.75: under-coupled, shallow low-band dip; 2.5: over-coupled, degraded match; 2.0: deepest notch and widest −10 dB span at 3.1–3.6 GHz, preserves X-band dip	2.0 mm	Best conjugate match near 3.45 GHz; maintains high-band integrity
Partial-ground height m (mm)	8, 9, 10	Ground return / effective electrical length	10: shifts low band upward and weakens match; 8: shifts down but narrows BW; 9: balanced resonance and −10 dB bandwidth	9 mm	Centers low band near 3.45 GHz with strong $\|S_{11}\|$ while keeping high-band stable
Step length f (mm)	7.5, 8.0, 8.5	Sets added low-band resonance	7.5: under-tuned, shallow low-band dip; 8.5: slight over-tune; 8.0: deepest low-band notch	8.0 mm	Opens/strengthens low-band resonance without detuning X-band
Step width g (mm)	1.0, 1.8, 2.5	Perturbs high-band current path	2.5: detunes/shallows high-band dip (11–12.5 GHz); 1.0: less coupling gain; 1.8: deepest high-band notch	1.8 mm	Maximizes $\|S_{11}\|$ depth at ~11.45 GHz while keeping low-band wide
Taper diagonal i (mm)	7.5, 8.0, 8.5	Coupling balance across bands	Moving away from 8.0 slightly reduces $\|S_{11}\|$ minima and narrows −10 dB spans; frequency centers largely unchanged	8.0 mm	Preserves dual deep notches and composite bandwidth

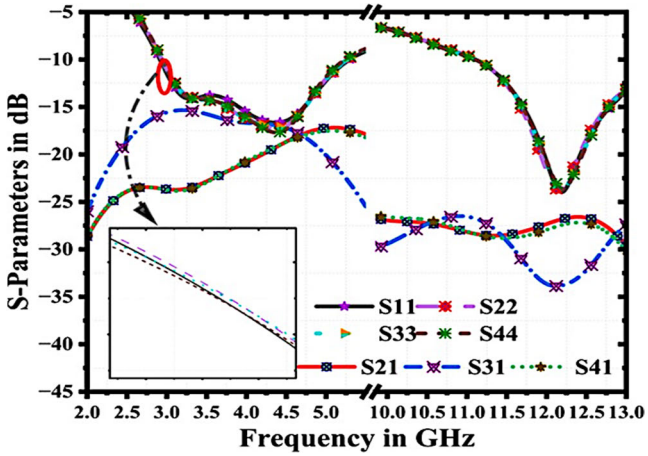

FIGURE 10. Simulated 4-port MIMO antenna with separate grounds.

3.055 GHz to 5.10 GHz, centered at 4.22 GHz, with excellent impedance matching characterized by a return loss of −47.25 dB at resonance. This configuration enhances the operational bandwidth and effectively suppresses mutual coupling, with S_{21} remaining below −15.65 dB throughout the lower frequency range.

In the higher frequency band, the antenna operates from 10.45 GHz to beyond 13 GHz, with a resonance at 11.60 GHz and an S_{xx} value of –23.85 dB. The mutual coupling (S_{xy}) ranges between –24.90 dB and –28.10 dB, indicating effective isolation and stable performance across the band. Figure 12(a) displays the fabricated 4-port MIMO antenna prototype, including both top and bottom views, whereas

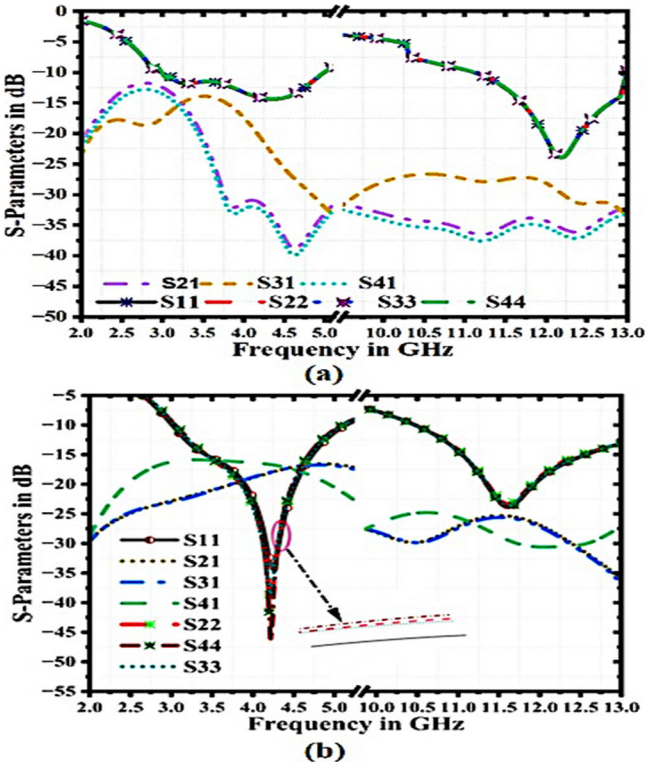

FIGURE 11. Simulated 4-port MIMO antenna with ground evolution: (a) Defected substrate and ground structure, and (b) Vertical slot integrated into the ground.

Figure 12(b) shows the measurement setup inside the anechoic chamber.

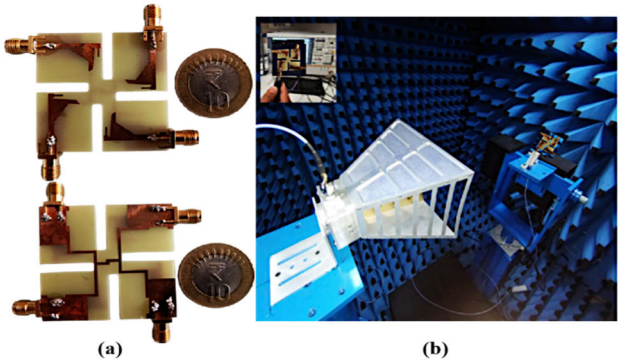

FIGURE 12. Prototype of the Proposed MIMO Antenna: (a) Front and rear views and (b) Anechoic chamber setup for antenna testing

In the higher frequency band, the antenna operates from 10.45 GHz to beyond 13 GHz, with a resonance at 11.60 GHz and an S_{xx} value of –23.85 dB. The mutual coupling (S_{xy}) ranges between –24.90 dB and –28.10 dB, indicating effective isolation and stable performance across the band. Figure 12(a) displays the fabricated 4-port MIMO antenna prototype, including both top and bottom views, whereas Figure 12(b) shows the measurement setup inside the anechoic chamber.

Figure 13 presents the simulated and experimental S-parameters (S_{11} and S_{21}) of the quad-port MIMO antenna, validating its dual-band operation across both low and high frequency regions. In the lower band, the simulated input reflection coefficient indicates effective matching between 2.71 GHz and 4.45 GHz, with the lowest S_{11} recorded as −27.50 dB at 3.16 GHz. The isolation parameter, S_{21}, stays below −16.25 dB, reflecting low mutual coupling. Measured data confirm a −10 dB impedance bandwidth of 1.65 GHz, ranging from 2.75 GHz to 4.40 GHz, with observed S_{11} and S_{21} values of −27 dB and less than −15.85 dB, respectively, at 3.16 GHz. These results align closely with the simulations. For the higher band, simulated bandwidth spans 10.45 GHz to 13 GHz (≈2.55 GHz), while measurements show a slightly narrower range from 10.45 GHz to 12.95 GHz. At 11.50 GHz, a minimum S_{11} of −38.62 dB is achieved, confirming strong impedance matching. S_{21} values of −24.75 dB (simulated) and −23.45 dB (measured) further confirms excellent isolation, supporting the antenna's viability for high-frequency MIMO systems.

IV. DIVERSITY PARAMETERS

This section presents a detailed analysis of these diversity parameters, demonstrating that the obtained simulation and measurement results achieve favorable values, thereby enhancing the overall diversity performance of the MIMO antenna system.

A. ECC quad-port AND DGquad-port

Figure 14 shows the simulated and measured results of the ECCquad-port and DGquad-port for the quad-port MIMO antenna configured for dual-band operation. The theoretical

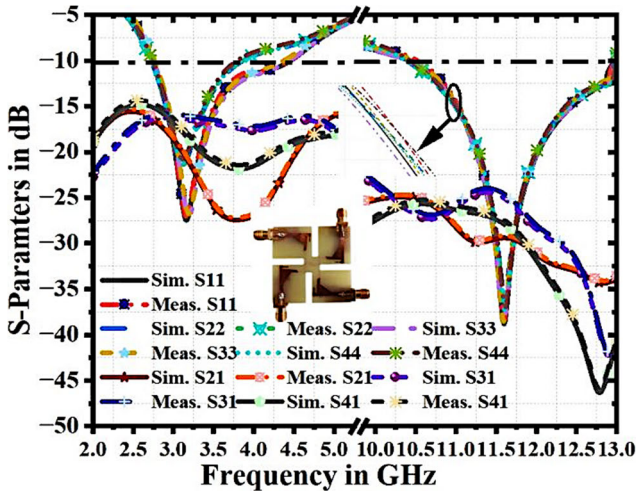

FIGURE 13. Simulated and measured S_{xx} and S_{xy} results of the proposed 4-port MIMO antenna.

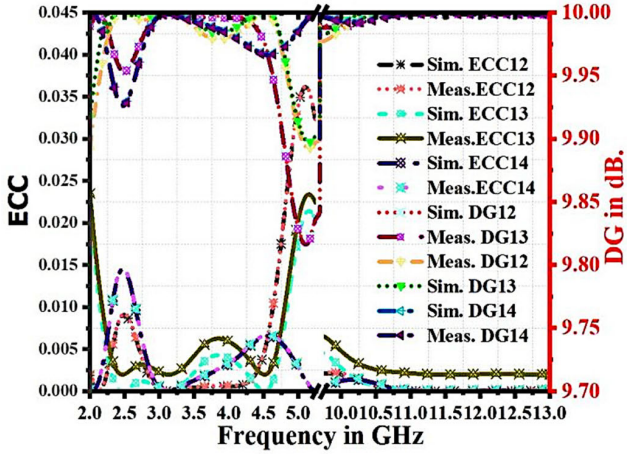

FIGURE 14. Computed and experimental $ECC_{quad-port}$ and $DG_{quad-port}$ results for the proposed 4-port MIMO antenna.

calculations of $ECC_{quad-port}$ and $DG_{quad-port}$ are shown in Equations 4 and 5 [5].

$$ECC = \frac{\left|S_{ii}^{*}S_{ij} + S_{ij}^{*}S_{jj}\right|^{z}}{\left(1-\left|S_{ii}\right|^{z} - \left|S_{ij}\right|^{z}\right)\left(1-\left|S_{jj}\right|^{z} - \left|S_{ij}\right|^{z}\right)} \quad (4)$$

$$DG = 10\sqrt{1-\left|ECC\right|^{z}} \quad (5)$$

The computed $ECC_{quad-port}$ values for the proposed quad-port configuration are consistently low, remaining under 0.005 in simulations and below 0.006 in experimental validation for the lower frequency range. For the same band, the $DG_{quad-port}$ exceeds 9.99 dB in simulation and is recorded at approximately 9.966 dB in measurements. In the upper frequency band, $ECC_{quad-port}$ remains minimal with simulated and measured values of 0.0020 and 0.0023, respectively. The corresponding $DG_{quad-port}$ is maintained close to the theoretical maximum, measured around 10 dB, indicating excellent isolation and diversity performance across operating bands.

B. $TARC_{quad-port}$, $MEG_{quad-port}$, AND $CCL_{quad-port}$

The theoretical assessment of diversity performance, which includes $TARC_{quad-port}$, $MEG_{quad-port}$, and $CCL_{quad-port}$, uses Equations (6)–(8). For TARCquad-port and $MEG_{quad-port}$, the best values should be below 0 dB, usually between −3 dB and −12 dB, while for $CCL_{quad-port}$, it should be 0.45 bits/sec/Hz. Figures 15 to 17 illustrate the simulated and experimental results for the proposed quad-port MIMO antenna. As presented in Fig. 15, both simulated and measured $MEG_{quad-port}$ values fall within the range of −3 dB to −3.28 dB in the low- and high-frequency regions. For $TARC_{quad-port}$, the simulated curves remain below −9 dB and −10 dB, while corresponding measured values are slightly higher at −8.9 dB and −9.75 dB across the respective operating bands, as shown in Fig. 16. The $CCL_{quad-port}$ characteristics in Fig. 17 show that the system performs very well, with values between 0.017 and 0.3715 bits/sec/Hz in the lower band (sub-6GHz) and from 0.312 to 0.0404 bits/sec/Hz in the higher frequency band. These findings validate the antenna's capability to maintain low correlation and support efficient MIMO performance across dual-band operation.

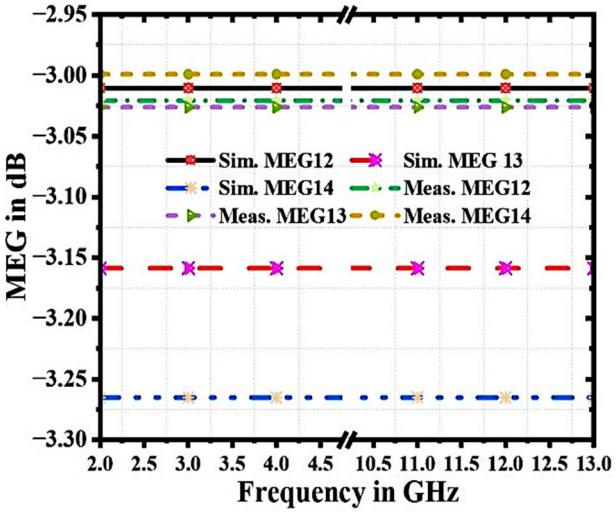

FIGURE 15. Computed and experimental $MEG_{quad-port}$ results for the proposed 4-port MIMO antenna.

$$TARC(\Gamma) = \sqrt{\frac{\sum_{i=1}^{N}\left|S_{ii} + \sum_{j\neq 1} S_{ij}e^{j\theta_j}\right|^2}{N}} \tag{6}$$

$$MEG_{\frac{i}{j}} = 0.50\left[1 - \sum_{\substack{i=1\\ i}}^{N}\left|S_{ij}\right|^2\right] < -3dB \tag{7}$$

$$CCL = -log_2 \det(A) \tag{8}$$

Here

$$A = \begin{bmatrix} a_{11} & \cdot & a_{14} \\ \cdot & \cdot & \cdot \\ a_{41} & \cdot & a_{44} \end{bmatrix}$$

$$a_{ii} = 1 - \left(|S_{ii}|^2 + |S_{ij}|^2\right.$$

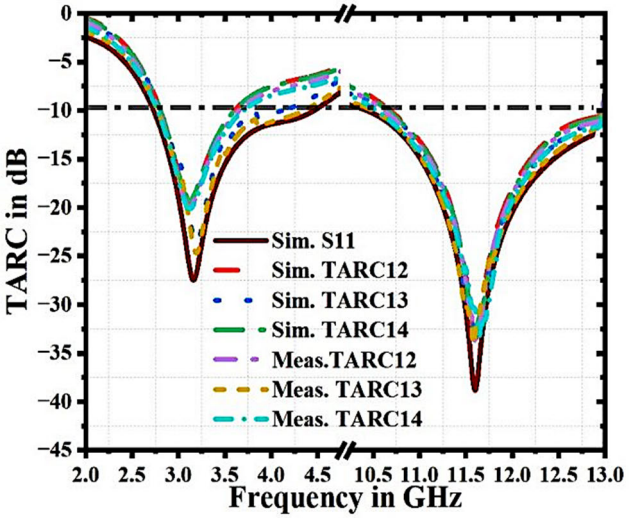

FIGURE 16. Simulated and measured TARC quad-port results of the proposed 4-port MIMO antenna.

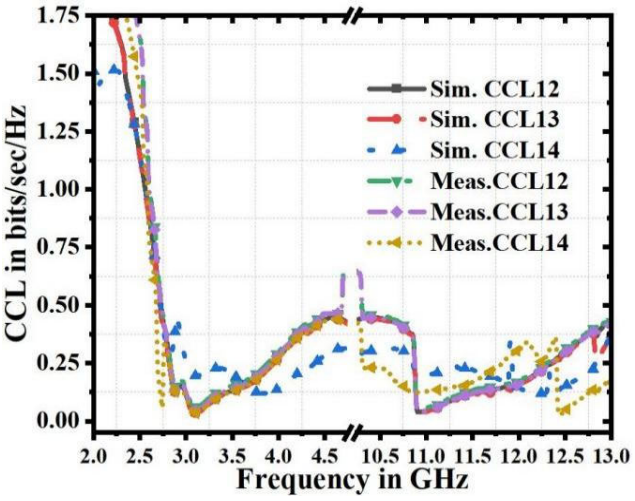

FIGURE 17. Computed and experimental $CCL_{quad-port}$ results for the proposed 4-port MIMO antenna.

$$a_{ij} = \left(S_{ij}^*, S_{ij}, +S_{ji}, S_{jj}^*\right), \text{ for i, j} = 1 \text{ to } 4$$

Figure 18 presents the gain and radiation efficiency results obtained through both simulation and measurement. In the lower frequency band, the antenna achieves a simulated peak gain of 3.25 dBi, closely aligning with the measured value of 3.15 dBi. At higher frequencies, the peak gain reaches 4.5 dBi in simulations and 4.35 dBi in experimental results. Radiation efficiency varies between 70% and 81% across the lower band, while the upper band exhibits effectiveness ranging from 72% to 84%.

Figure 19 displays both simulated and measured 2D radiation patterns for the four-port MIMO antenna at 3.14 GHz and 11.45 GHz, encompassing co-polarization and cross-polarization components. The evaluation is conducted in a spherical coordinate framework, where the angles θ and φ map to the XZ and YZ planes, respectively. When $\varphi = 0°$, the variation of θ corresponds to the

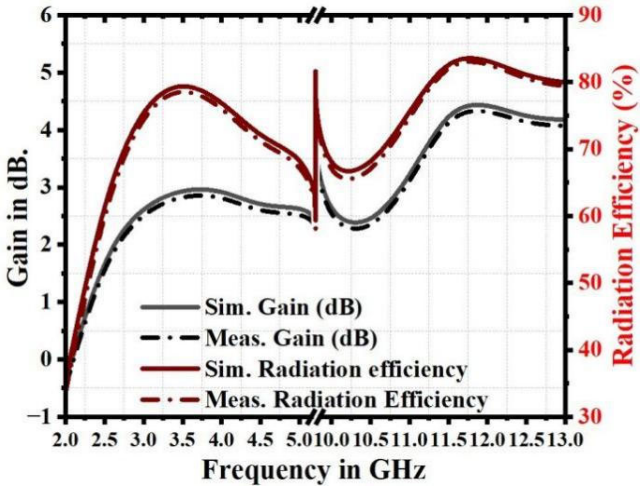

FIGURE 18. Comparison between simulated and measured results for (a) peak gain (in dBi) and (b) radiation efficiency (in %).

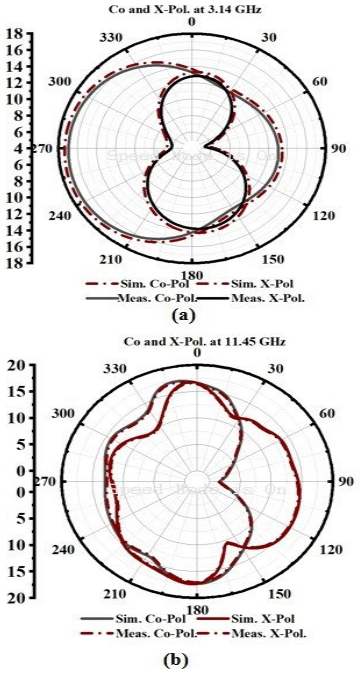

FIGURE 19. Co (XZ-Plane)- and X-Pol (YZ-Plane). Characteristics of simulated and measured 2D radiation patterns of Port 1 at (a) 3.14 GHz and (b) 11.45 GHz.

E-plane (XZ-plane), while $\varphi = 90°$ represents the H-plane (YZ-plane).

The observed patterns reveal stable and omnidirectional radiation characteristics, confirming the antenna's effectiveness in providing wide-angle coverage and reliable MIMO performance. Figure 20 presents the 3D radiation patterns of the quad-port MIMO antenna, confirming stable omnidirectional behavior across all ports. The orthogonal arrangement of the radiating elements enhances spatial diversity and contributes to improved MIMO performance. Resonance is observed at 3.14 GHz in the sub-6 GHz band and at 11.45 GHz within the X-band for each port.

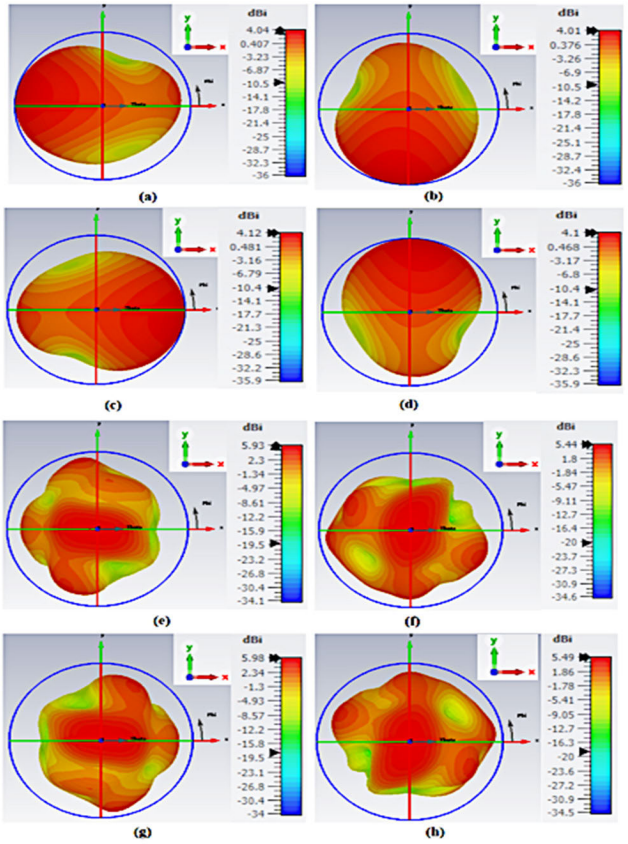

FIGURE 20. Simulated 3D far-field radiation patterns of the proposed MIMO antenna at 3.14 GHz and 11.45 GHz: (a), (e) Port 1; (b), (f) Port 2; (c), (g) Port 3; and (d), (h) Port 4.

The proposed four-port tapered and stepped dual-wideband MIMO antenna offers significant performance improvements over existing designs. With a compact footprint of 44 × 44 × 1.6 mm^3, it achieves substantial miniaturization while supporting dual-wideband operation from 2.72–4.45 GHz and 10.33–13 GHz, covering both sub-6 GHz and X-band applications. The use of a defected ground structure (DGS) combined with self-isolation techniques ensures superior inter-port isolation of –16.25 dB to –25 dB without the need for additional decoupling networks, which often increase the size and complexity of comparable designs [18], [28], [32]. Compared to larger counterparts [20], [36], [37], [38], [39], [40], [41], [42], [43], the proposed design provides higher isolation, broader bandwidth, and a more compact form factor. It maintains high radiation efficiency (72–84%) and stable peak gain (3.3–4.5 dBi) across both bands, with excellent diversity performance parameters

including ECC $\leq$ 0.005, DG $\approx$ 10 dB, TARC $\leq$ –9.5 dB, and CCL $\leq$ 0.35 bits/s/Hz. The unified connected ground structure, unlike the separate or partially connected grounds used in some prior works [39], enhances mechanical robustness, eases integration into compact platforms, and effectively suppresses mutual coupling, as discussion in Table 2. These combined features make the antenna strong candidate for multi-standard wireless systems such as 5G NR, DTH, and satellite communications.

TABLE 2. Benchmarking of the proposed antenna against cutting-edge designs.

Ref./Ports/ Year	Size (mm^3)	Freq. Band (GHz)	Isolation (S_{21})	Peak Gain (dBi)	Radiation Efficiency (%)	ECC/ DG (dB)	TARC (dB)	MEG (dB)	CCL (bp/s/Hz)	Applications	CG	Techniques
[36]/4 , 2023	53×42×1.6	3.3–3.8, 4.5–8.4	10	0.3 – 3.5	60–80	0.005/ -	-	-	-	S6G, X-B	No	Tap. feed, DGS
[37]/4 , 2024	41×41×1.6	2–19	25.5	8	89	0.02/ 10	-10	-	0.25	S6G, X-B	No	Self-coup., DGS, meta.
[38]/4 , 2025	65×65×0.1	3.3–4.5, 4.9–7.3, 8.1–11	25	7	80–90	0.01/ 9.99	-10	-	0.38	S6G, X-B	Yes	CPW, Decoup. elem.
[39]/4 , 2024	40×40×1.6	3-13.5	20	1.9 8	80	0.005/ 10	-	0.2	0.1	S6G, X-B	Yes	Part. ground isol.
[40]/4 , 2024	50×50×1.6	3.33-5.04	23	2.5	87	0.05/ 10	-10	-	0.32	S6G	No	Meta. Super.
[41]/4 , 2025	64×32×0.78 7	5.0-50	40	6.1	-	0.03/ 9.99	-20	-4	0.14	X-B, mm-wave	No	Self-coup., DGS
[20]/4 , 2024	78×64.5×1.6	2.7-4.2	22	4.4	98	0.00789/ 9.96	-15	0.005	0.24	S6G	Yes	T-shape DE
[42]/4 , 2024	58×58×1.6	3.1-4.2	15	3-4	90	0.0001/ 9.99	-10	-3.08	0.02	S6G	No	Def. Substr.
[43]/4 , 2024	56×56×1.6	3.25-3.90,4.36 -4.93	15	2.5 9	90	0.0005/ 10	-10	-3.08	0.05 2	S6G	No	Def. Substr.
PMA /4	**44×44×1.6**	**2.72-4.45, 10.33–13**	**16.25 , 25**	**3.3, 4.5**	**72-84**	**0.005, 0.002/ 9.9, 10**	**-9.5-10**	**-3.15**	**0.35, 0.25**	**S6G, X-B**	**Yes**	**DGS, Def. Substr.**

S6G: Sub-6 GHz, X-B: X-Band, Def. Substr: defected substrate, CG: Connected Ground, PMA: Proposed MIMO Antenna

The design parameters are carefully optimized to cover 2.72–4.45 GHz (sub-6 GHz) and 10.33–13 GHz (X-band), ensuring full compatibility with the n77, n78, and n79 5G-NR bands. The proposed antenna demonstrates strong electromagnetic performance with $S_{11} < -10$ dB, ECC ≤ 0.005, DG ≈ 10 dB, TARC ≤ -9.5 dB, and CCL ≤ 0.35 bits/s/Hz across the operational bands. It maintains high radiation efficiency (72–84%) and stable peak gain (3.3–4.5 dBi), ensuring reliable mid-band 5G performance. The unified connected ground structure enhances mechanical robustness, simplifies integration into compact devices, and effectively suppresses mutual coupling, unlike the separate or partially connected grounds used in earlier designs [39], as summarized in Table 2. These combined features establish the proposed antenna as a strong candidate for multi-standard wireless platforms, including 5G-NR, DTH, and satellite communication systems.

V. CONCLUSION

This study presents a compact four-port MIMO antenna system with overall dimensions of $44 \times 44 \times 1.6$ mm^3. The design employs a modified rectangular radiating patch integrated with a uniquely tapered and stepped monopole-inspired structure. It incorporates a defected ground and defected substrate configuration combined with spatial diversity techniques to enhance isolation. This approach not only preserves but also optimizes the dual operating bandwidths, effectively covering 2.72–4.45 GHz and 10.33–13 GHz. The microstrip-fed MIMO antenna demonstrates robust diversity performance, achieving $ECC_{quad-port}$ <0.005,

$DG_{quad-port}$ ≈10 dB, and $CCL_{quad-port}$ <0.35 bps/Hz. The $MEG_{quad-port}$ is –3.0 dB, while the $TARC_{quad-port}$ remains around –10 dB. The antenna exhibits high radiation efficiency between 72% and 84%, with peak gain values ranging from 3.50 to 4.50 dBi. The consistency between simulated and measured 2D radiation patterns confirms stable omnidirectional radiation characteristics across the principal planes. The proposed antenna's compact single-layer structure with a unified ground plane provides mechanical robustness, PCB process compatibility, and ease of fabrication, making it well suited for real-world deployment. Furthermore, its dual-band operation extends applicability across 5G NR and X-band systems, supporting vehicular (V2X) and satellite communication links. These attributes establish the proposed design as a strong candidate for next-generation wireless systems,

including 5G NR bands n77/n78/n79 and X-band services, suitable for smartphones, IoT gateways, vehicular modules, and small-cell base stations.

REFERENCES

[1] A. A. Yussuf and S. Paker, "Design of wideband MIMO antenna for wireless applications," in *Proc. 25th Signal Process. Commun. Appl. Conf. (SIU)*, May 2017, pp. 1–4.

[2] I. Rashid, A. Rauf, and F. A. Bhatti, "A novel UWB MIMO antenna array with band notch characteristics using parasitic decoupler," *J. Electromagn. Waves Appl.*, vol. 34, no. 9, pp. 1225–1238, Jun. 2020.

[3] S. Kumar, A. S. Dixit, R. R. Malekar, H. D. Raut, and L. K. Shevada, "Fifth generation antennas: A comprehensive review of design and performance enhancement techniques," *IEEE Access*, vol. 8, pp. 163568–163593, 2020.

[4] A. Abbas, N. Hussain, M. A. Sufian, J. Jung, S. M. Park, and N. Kim, "Isolation and gain improvement of a rectangular notch UWB-MIMO antenna," *Sensors*, vol. 22, no. 4, p. 1460, Feb. 2022.

[5] M. Srinubabu and N. V. Rajasekhar, "Enhancing diversity and isolation performance for a four-port MIMO antenna in FR-1 5G frequency bands," *IETE J. Res.*, vol. 70, no. 8, pp. 1–16, Aug. 2024.

[6] S. Manumula and N. V. Rajasekhar, "Design of compact MIMO antenna for 5G applications," in *Proc. 3rd Int. Conf. Artif. Intell. Signal Process. (AISP)*, Mar. 2023, pp. 1–5.

[7] M. Fuentes, J. L. Carcel, C. Dietrich, L. Yu, E. Garro, V. Pauli, F. I. Lazarakis, O. Grøndalen, Ö. Bulakci, J. Yu, W. Mohr, and D. Gomez-Barquero, "5G new radio evaluation against IMT-2020 key performance indicators," *IEEE Access*, vol. 8, pp. 110880–110896, 2020.

[8] M. Srinubabu and N. V. Rajasekhar, "A compact and efficiently designed two-port MIMO antenna for N78/48 5G applications," *Heliyon*, vol. 10, no. 7, Apr. 2024, Art. no. e28981.

[9] S. Ahmad, S. Khan, B. Manzoor, M. Soruri, M. Alibakhshikenari, M. Dalarsson, and F. Falcone, "A compact CPW-fed ultra-wideband multi-input-multi-output (MIMO) antenna for wireless communication networks," *IEEE Access*, vol. 10, pp. 25278–25289, 2022.

[10] M. Srinubabu and N. V. Rajasekhar, "Design and analysis of a compact 4-port MIMO antenna for improved isolation and 5G (n78/n77/n48) performance," *Traitement du Signal*, vol. 41, no. 4, pp. 2057–2067, Aug. 2024.

[11] R. Chataut and R. Akl, "Massive MIMO systems for 5G and beyond networks—Overview, recent trends, challenges, and future research direction," *Sensors*, vol. 20, no. 10, p. 2753, May 2020.

[12] J. K. Rai, P. Ranjan, and R. Chowdhury, "Dual-band high tuning range frequency reconfigurable cylindrical dielectric resonator antenna for n7, n30, n38, n40, n41, n46, n47, n53 and n79 5G new radio application with machine learning approach," *Arabian J. for Sci. Eng.*, vol. 50, no. 14, pp. 1–11, Jul. 2025.

[13] N. Maziar, W. Yue, T. Milos, W. Shangbin, Q. Yinan, and A.-I. Mohammed, "Overview of 5G modulation and waveforms candidates," *J. Commun. Inf. Netw.*, vol. 1, no. 1, pp. 44–60, Jun. 2016.

[14] V. Rajavel and D. Ghoshal, "Multiband antenna design with integrated amc surface and fss superstrate for wireless body area network communications," *Arabian J. Sci. Eng.*, vol. 49, no. 12, pp. 16495–16520, 2024.

[15] J. K. Rai, P. Ranjan, and R. Chowdhury, "Dual band high tuning range frequency reconfigurable dielectric resonator antenna for sub-6 GHz applications," *Int. J. Electron. Lett.*, vol. 13, no. 1, pp. 47–55, Jan. 2025.

[16] M. Srinubabu and N. V. Rajasekhar, "A compact and highly isolated integrated 8-port MIMO antenna for sub-6 GHz and mm-Wave 5G-NR applications," *Results Eng.*, vol. 25, Mar. 2025, Art.s no. 104068.

[17] S. Ghosh, G. S. Baghel, and M. V. Swati, "Design of a highly-isolated, high-gain, compact 4-port MIMO antenna loaded with CSRR and DGS for millimeter wave 5G communications," *AEU-Int. J. Electron. Commun.*, vol. 169, Sep. 2023, Art. no. 154721.

[18] D. M. John, S. Vincent, K. Nayak, B. Supreetha, T. Ali, P. Kumar, and S. Pathan, "A compact flexible four-element dual-band antenna using a unique defective ground decoupling structure for sub-6 GHz wearable applications," *Results Eng.*, vol. 21, Mar. 2024, Art. no. 101900.

[19] E. Saenz, K. Guven, E. Ozbay, I. Ederra, and R. Gonzalo, "Decoupling of multifrequency dipole antenna arrays for microwave imaging applications," *Int. J. Antennas Propag.*, vol. 2010, no. 1, 2010, Art. no. 843624.

[20] G. Tangirala, S. Garikipati, M. K. Meshram, M. K. C. Durbhakula, and V. K. Sharma, "Quad element luna-shaped UWB-MIMO antenna with improved isolation and gain using novel decoupling networks," *Wireless Netw.*, vol. 30, no. 4, pp. 2557–2569, May 2024.

[21] M. Cholavendan and V. Rajeshkumar, "Dual-feed orthogonally polarized compact 8-element MIMO antenna using metallic stub and decoupling unit for isolation enhancement of sub-6 GHz 5G application," *Prog. Electromagn. Res. Lett.*, vol. 116, pp. 105–111, 2024.

[22] Z. Li, Z. Du, M. Takahashi, K. Saito, and K. Ito, "Reducing mutual coupling of MIMO antennas with parasitic elements for mobile terminals," *IEEE Trans. Antennas Propag.*, vol. 60, no. 2, pp. 473–481, Feb. 2012.

[23] G. Tamminaina and R. Manikonda, "Investigation on performance of four port MIMO antenna using electromagnetic band gap for 5G communication," *Prog. Electromagn. Res. M*, vol. 119, pp. 51–62, 2023.

[24] A. Raj and D. Mandal, "Design and analysis of graphene-based PBG and EBG array antennas for wideband and multiband mm-Wave applications," *Waves Random Complex Media*, pp. 1–35, 2024, doi: 10.1080/17455030.2024.2415935.

[25] R. H. Elabd and A. A. Megahed, "Isolation enhancement of a two- orthogonal printed elliptical slot MIMO antenna array with EBG structure for millimeter wave 5G applications," *Discover Appl. Sci.*, vol. 6, no. 5, p. 222, Apr. 2024.

[26] W. F. A. Mshwat, J. S. Kosha, A. Salisu, A. Ullah, N. T. Ali, I. Elfergani, C. H. See, C. Zebiri, J. Rodriguez, and R. Abd-Alhameed, "Compact reconfigurable MIMO antenna for 5G and Wi-Fi applications," *IEEE Access*, vol. 12, pp. 110283–110298, 2024.

[27] A. Raj and D. Mandal, "Design and performance analysis of dielectric resonator antenna array for 5G mm-Wave ground-based navigation and wireless applications," *Arabian J. for Sci. Eng.*, vol. 50, no. 14, pp. 1–30, Jul. 2025.

[28] A. Desai, H.-T. Hsu, Y.-F. Tsao, B. M. Yousef, and A. A. Ibrahim, "FSS based high gain optically transparent MIMO antenna for sub-6 GHz 5G mid-band applications," *Optik*, vol. 307, Jul. 2024, Art. no. 171829.

[29] X. Peng and C. Du, "A flexible CPW-fed tri-band four-port MIMO antenna for 5G/WiFi 6E wearable applications," *AEU-Int. J. Electron. Commun.*, vol. 174, Jan. 2024, Art. no. 155036.

[30] M. F. A. Sree, M. H. A. Elazeem, and W. Swelam, "Dual band patch antenna based on letter slotted DGS for 5G sub-6 GHz application," *J. Phys., Conf. Ser.*, vol. 2128, no. 1, Dec. 2021, Art. no. 012008.

[31] G. N. J. Sree, K. V. Babu, S. Das, and T. Islam, "Design and optimization of a deep learning algorithm assisted stub-loaded dual band four-port MIMO antenna for sub-6 GHz 5G and x band satellite communication applications," *AEU-Int. J. Electron. Commun.*, vol. 175, Feb. 2024, Art. no. 155074.

[32] A. Ali, M. Rasool, M. Z. Zahid, I. Rashid, A. M. Siddique, M. Maqsood, and F. A. Bhatti, "A 4-port broadband high-isolated MIMO antenna for wireless communication," *Prog. Electromagn. Res. C*, vol. 142, pp. 119–130, 2024.

[33] P. Sharma, R. N. Tiwari, P. Singh, and B. K. Kanaujia, "Dual-band trident shaped MIMO antenna with novel ground plane for 5G applications," *AEU-Int. J. Electron. Commun.*, vol. 155, Oct. 2022, Art. no. 154364.

[34] B. Bukhari and G. M. Rather, "4-port MIMO antenna for sub-1 GHz, IoT, and sub-6 GHz 5G new radio applications," *Prog. Electromagn. Res. C*, vol. 127, pp. 113–125, 2022.

[35] M. S. Sharawi, "Current misuses and future prospects for printed multiple-input, multiple-output antenna systems [wireless corner]," *IEEE Antennas Propag. Mag.*, vol. 59, no. 2, pp. 162–170, Apr. 2017.

[36] N. Salim, M. S. J. Singh, A. T. Abed, and M. T. Islam, "4×4 MIMO slot antenna spanner shaped low mutual coupling for Wi-Fi 6 and 5G communications," *Alexandria Eng. J.*, vol. 78, pp. 141–148, Sep. 2023.

[37] M. A. Rahman, S. S. Al-Bawri, W. M. Abdulkawi, K. Aljaloud, and M. T. Islam, "A unique SWB multi-slotted four-port highly isolated MIMO antenna loaded with metasurface for IoT applications-based machine learning verification," *Eng. Sci. Technol., Int. J.*, vol. 50, Feb. 2024, Art. no. 101616.

[38] C. Du, F. Zhang, and R. Li, "Design of tri-band flexible CPW 4-port slot MIMO antenna for conformal 5G, WiFi 6/6E and X-band applications," *Eng. Sci. Technol., Int. J.*, vol. 62, Feb. 2025, Art. no. 101937.

[39] K. Pandya, T. Upadhyaya, U. Patel, V. Sorathiya, A. Pandya, A. J. A. Al-Gburi, and M. M. Ismail, "Performance analysis of quad-port UWB MIMO antenna system for sub-6 GHz 5G, WLAN and x band communications," *Results Eng.*, vol. 22, Jun. 2024, Art. no. 102318.

[40] I. Khan, K. Zhang, L. Ali, and Q. Wu, "Enhanced quad-port MIMO antenna isolation with metamaterial superstrate," *IEEE Antennas Wireless Propag. Lett.*, vol. 23, pp. 439–443, 2024.
[41] L. Matta, B. Sharma, and M. Sharma, "Experimental analysis of four-port MIMO multi-band bandwidths antenna within two wide-bands (6.88–21.23 GHz & 27.95–44.66 GHz) with high isolation for future wearable applications," *Wireless Netw.*, vol. 31, pp. 2525–2553, Apr. 2025.
[42] T. Addepalli, G. N. Kumar, C. J. Rani, N. Koppala, C. R. Jetti, C. M. Kumar, R. Uppada, and B. K. Kumar, "A defected substrate 4-element MIMO antenna with higher diversity characteristics for 5G sub 6 GHz N77/N78 band applications," *Wireless Netw.*, vol. 31, no. 2, pp. 1–17, Feb. 2025.
[43] T. Addepalli, M. Sharma, M. S. Kumar, G. Naveen Kumar, P. R. Kapula, and C. M. Kumar, "Self-isolated miniaturized four-port multiband 5G sub 6 GHz MIMO antenna exclusively for n77/n78 & n79 wireless band applications," *Wireless Netw.*, vol. 30, no. 2, pp. 1037–1053, Feb. 2024.
[44] T. Addepalli, "Effective area reduction & surface waves suppression of a novel four-element MIMO antenna exclusively designed for dual band 5G sub 6 GHz (N77/N78 & N79) applications," *Wireless Netw.*, vol. 31, no. 2, pp. 1463–1479, Feb. 2025.

BHASKARA RAO PERLI received the B.Tech. and M.Tech. degrees in electronics and communication engineering from the Jawaharlal Nehru Technological University College of Engineering, Hyderabad, India, in 2005 and 2011, respectively, and the Ph.D. degree from JNTUA, Anantapur. He is currently an Associate Professor with the Department of ECE, St. Ann's College of Engineering and Technology, Chirala, Andhra Pradesh, India. He has published six SCI indexed journals, five Scopus-indexed journals, six international conferences presented. His research interests include characteristic mode analysis (CMA), wideband antennas, microwave antennas, millimeter antennas, and wireless communications.

TATHABABU ADDEPALLI was born in Andhra Pradesh, India. He received the B.Tech. degree from JNTUH, Hyderabad, in 2007, the M.Tech. degree from JNTUK, Kakinada, Andhra Pradesh, in 2010, and the Ph.D. degree from JNTUA, Anantapur, in 2022.

Currently, he is an Associate Professor with the Department of ECE, Aditya Engineering College (A), Surampalem, Kakinada. He has published 34 SCIE papers, six Scopus indexed papers, and nine papers presented in international conferences. He attended more than 40 workshops related to antennas and wireless communications in various reputed institutions. The articles are published in various reputed international journals, such as IEEE Access (IEEE), *International Journal of Electronics and Communications* (AEU, Elsevier), *Alexandria Engineering Journal* (AEJ, Elsevier), *International Journal of Communication Systems* (IJCS, Wiley), *Transaction on Emerging Telecommunication Technologies* (ETT, Wiley), *Electronics* (MDPI), *Micromachines* (MDPI), *Wireless Personal Communications* (WPC, Springer), *Wireless Networks* (WN, Springer), *Journal of Electromagnetic Waves and Applications* (JEMWA, Taylor & Francis), and *IETE Journal of Research* (IETE, Taylor & Francis), presented nine papers in conferences (eight IEEE and one Springer), published two book chapter on THz antennas and planar microstrip antennas and published four patents. His areas of interest are microstrip patch antennas, MIMO antennas, 5G antennas (sub 6 GHz and mmWave), UWB Antennas, flexible antennas, characteristic mode analysis (CMA), THz antennas, and metamaterial antennas. He is a reviewer for reputed journals, such as *IJCS*, *PIER*, *Electronics*, *Telecommunication Systems*, *AEU*, and *Journal of Infrared, Millimeter, and Terahertz Waves*.

MANUMULA SRINUBABU received the B.Tech. degree in electronics and communication engineering and the M.Tech. degree in VLSI and embedded systems from JNTUK, Kakinada, in 2008 and 2016, respectively, and the Ph.D. degree in RF and microwave engineering with VIT-AP University, Andhra Pradesh, India, in 2025. He is an Assistant Professor with the ECE Department, Aditya University, Surampalem, kakinada. From 2021 to 2025, he was a full-time Research Scholar with VIT-AP University. He has published over seven SCI-indexed journal articles with reputed publishers, presented more than three papers at international conferences, and holds two patents. His research interests include the development of 5G MIMO antennas and planar antennas.

SIVASUBRAMANYAM MEDASANI (Senior Member, IEEE) received the B.Tech. degree in electronics and communication engineering, the M.Tech. degree in digital electronics and communication systems, and the Ph.D. degree in microwave remote sensing from the Sri Venkateshwara University College of Engineering, Sri Venkateshwara University, Tirupati, India, in 2005, 2012, and 2020, respectively. He is currently a Professor with the Department of CSE, K. S. School of Engineering and Management, Bengaluru, India. His research mainly focuses on microwave remote sensing, radar data processing, electromagnetics, antennas, microwaves, photonics, electron devices and VLSI. He is a Individual Member of ISPRS, a Life Member of ISTE and ISRS, and a member of Institution of Engineers (India) and IETE.

PADMAJA NIMMAGADDA received the B.E. degree in ECE from the University of Mumbai, India, and the M.Tech. (Hons.) and Ph.D. degrees in the area of atmospheric radar signal processing from Sri Venkateshwara University, in 2003 and 2012, respectively. Currently, she is a Professor of ECE and the Deputy Dean of innovations, with the School of Engineering, Mohan Babu University (Erstwhile Sree Vidyanikethan Engineering College), Tirupati, India. She has 25 years of experience in Teaching, Research, Guiding, Mentoring, and Industrial collaboration. She is working for four projects funded by ISRO, DST, and AICTE worth 2.05 crores. She received appreciation as the Coordinator of Institution Innovation Council (IIC) for recognition as Best Performing IIC from MHRD at AICTE HQ's, New Delhi, in 2019. She served various administrative positions, such as the Head of the Department, the Coordinator for NBA, NAAC, MSME, AICTE IDEA Lab, Innovation Council, a Executive Council member, and a Treasurer of IETE, Tirupati Center, from 2012 to 2021. She has published more than 100 technical articles in various reputed international journals and contributed nine book chapters. She published seven patents; one patent is granted. Her areas of interests include signal and image processing and communication systems. She is a Life Member of ISTE, IETE, IAENG, ISCA, InSc, and IACSIT. She received the Best Teacher Award at C. R. Engineering College, the Best Citizens of India Award, and the Research Excellence Award 2020, and the Innovative Educator Award from the Institute of Scholars (InSc). She served as a technical session chairs and a technical program committee member and delivered key note address in various national and international conferences held in India and Singapore. She is also an editorial board member and a member of review panel for various journals and conferences.

C. RAJU received the B.Tech. and M.Tech. degrees in electronics and communication engineering from Jawaharlal Nehru Technological University Anantapur (JNTUA), Andhra Pradesh, India, in 2009 and 2012 respectively, and the Ph.D. degree in signal processing from Sri Venkateswara University, Tirupati, in 2019. He is currently a Professor with the Department of Electronics and Communication Engineering, Sri Venkateswara College of Engineering. His research focuses in the areas of radar signal processing, microwave remote sensing and image processing. He is a member of the Institutions of Engineer, a fellow of IETE, and a Life Member of ISTE.

MANISH SHARMA (Senior Member, IEEE) received the B.E. degree in electronics and communication engineering from Mangalore University, Karnataka, India, in 2000, the M.Tech. degree from Visvesvaraya Technological University, Karnataka, in 2007, and the Ph.D. degree from the Department of Electronics Engineering, Banasthali University, Rajasthan, India, in 2017. He is currently the Director and a Professor-Researcher with Chitkara University Research and Innovation Network (CURIN), Chitkara University, Punjab, India. He is guiding eight Ph.D. students with four scholars completed Ph.D. He is also the Founder–Director of Spectrum Wirelesscomm Pvt. Ltd., which provides solutions to healthcare and agricultural problems. He has published more than 179 research articles and granted with two utility and 30 design patents. He has also published 18 book chapters. His research interests include computational electromagnetics, reconfigurable antennas, novel electromagnetic materials, dielectric resonator antennas, wideband/super-wideband antennas, wideband/dual band/triple band microstrip antennas for wireless communication, smart and MIMO antennas systems, radio-frequency identification (RFID) antennas, antennas for healthcare, RF MEMS planar antenna on Si substrate, wireless networks, body area networks, meta surface-based biosensors, designing of microstrip antennas using machine learning and artificial network. He has also been featured in the list of 2% all over the world for the years 2021, 2022, 2023, and 2024, respectively, released by Stanford University, USA. He is also a reviewer of IEEE Access, *Journal of Electromagnetic Waves and Applications*, *AEU: International Journal of Electronics and Communication*, *International Journal of Communication Systems*, *International Journal of Microwave and Wireless Technologies*, *International Journal of RF and Microwave Computer-Aided Engineering*.

ZAHRILADHA ZAKARIA (Senior Member, IEEE) was born in Johor, Malaysia. He received the B.Eng. and M.Eng. degrees in electrical and electronic engineering from Universiti Teknologi Malaysia (UTM) in 1998 and 2004, respectively, and the Ph.D. degree in electrical and electronic engineering from the Institute of Microwaves and Photonics (IMP), University of Leeds, U.K., in 2010. He began his career with STMicroelectronics Malaysia from 1998 to 2002, as a Product Engineer before joining Universiti Teknikal Malaysia Melaka (UTeM), where he currently serves as the Deputy Vice Chancellor (Research and Innovation) and a Professor at the Microwave Research Group (MRG), Faculty of Electronic and Computer Engineering. He teaches courses in Microwave Engineering, Antenna and Propagation, Communication Principles, Wireless Communications, Electronic Systems, and Signal Processing. His research focuses on microwave device design and characterization, including planar and non-planar filters, resonators, amplifiers, and antennas, as well as microwave sensors, energy harvesting, and data communication systems for interdisciplinary applications. He has authored and co-authored over 400 scientific publications in journals, proceedings, and book chapters, and holds eight intellectual property rights. His innovative research has earned him numerous national and international awards, including gold medals at UTeMEX, Malaysia Technology Expo (MTE), International Invention, Innovation and Technology Exhibition (ITEX), International Trade Fair Ideas Inventions New Products (iENA, Germany), and the Seoul International Invention Fair (SiiF, Korea). A dedicated scholar and reviewer, he contributes actively to leading journals such as IEEE Transactions on Microwave Theory and Techniques, IEEE Sensors Journal, IEEE Access, IEEE Microwave and Wireless Components Letters, and IET Microwaves, Antennas and Propagation. He is also a Top Research Scientist Malaysia (TRSM 2021) and has been internationally recognized among the World's Top 2% Scientists (Stanford University and Elsevier, 2025).

AHMED JAMAL ABDULLAH AL-GBURI (Senior Member, IEEE) received the M.Eng. and Ph.D. degrees in electronics and computer engineering (telecommunication systems) from Universiti Teknikal Malaysia Melaka (UTeM), Malaysia, in 2017 and 2021, respectively. He is currently a Senior Lecturer with the Faculty of Electronic and Computer Engineering Technology, UTeM. He is also the Deputy Head of the Microwave Research Group (MRG) under the Centre for Telecommunication Research and Innovation (CeTRI), UTeM. He has authored and co-authored numerous papers in high-impact journals and international conference proceedings. His research interests include microwave sensors, metasurfaces, metamaterials, and MIMO antennas. He is a Registered Member of the Board of Engineers Malaysia (BEM), Malaysia Board of Technologists (MBOT), and the International Association of Engineers (IAENG). He has received the Best Paper Award from the IEEE Community and has earned several gold, silver, and bronze medals in both international and local innovation competitions. In 2023, 2024, and 2025, he was recognized among the world's top 2% of scientists by Stanford University, as published by Elsevier.